Local Heterogeneity for a Eu^{3+}-Doped Glass Evidenced by Time-Resolved Fluorescence Spectroscopy Coupled to Scanning Near-Field Optical Microscopy

Jérôme Grausem,[†] Manuel Dossot,*[,†] Sébastien Cremel,[†] Bernard Humbert,[†] François Viala,[‡] and Patrick Mauchien[‡]

Laboratoire de Chimie Physique et Microbiologie pour l'Environnement LCPME, UMR CNRS-UHP 7564, 405, rue de Vandoeuvre, F-54600 Villers-Les-Nancy, France, and CEA Saclay DEN/DANS/DPC/SCP, F-91191 Gif-Sur-Yvette, France

Received: February 3, 2006; In Final Form: March 31, 2006

Time-resolved fluorescence spectroscopy (TRFS) was applied to an aluminate glass sample doped with Eu^{3+} cation as a fluorescent probe of the chemical environment and local symmetry. Conventional far-field experiments revealed the presence of two different phases: an amorphous phase featured by a highly disordered environment surrounding the Eu^{3+} cation and a more ordered polycrystalline phase that exhibits a significant increase in the Eu^{3+} fluorescence decay time compared to that of the amorphous phase. Near-field fluorescence spectra and decay kinetics were recorded in the frontier region between the two phases using a home-built scanning near-field optical microscope. SNOM−TRFS experiments confirmed the presence of local heterogeneities in this part of the glass at a sub-micrometric spatial scale. Polycrystalline sites featured an important shear-force interaction with the probing fiber optic tip, a longer fluorescence decay time, and a higher Stark splitting of the $^5D_0 \rightarrow {}^7F_J$ ($J = 1-4$) electronic transitions of the Eu^{3+} cations.

1. Introduction

Interface phenomena between a solid sample and a fluid (gas or liquid) can be dramatically influenced by the heterogeneities of the solid surface, which include changes in morphology, structure, and/or composition. One has to understand how microscopic features are involved in the macroscopic properties of the sample to obtain a comprehensive description of the interface in terms of physicochemical properties. Spectroscopic methods are generally well adapted to probing the interface since they minimize perturbation. Vibrational and electronic spectroscopies are now designed for the collection of information at spatial resolution ranging from a few micrometers to the macroscopic scale. For instance, confocal microscopy has brought about significant improvement in the spatial resolution in fluorescence or Raman spectroscopy. However, these methods rely on traditional far-field optics and are intrinsically limited by the diffraction limit to a resolution of $\sim\lambda/2$, which at best corresponds to several hundreds of nanometers. This far-field limit obstructs the detection of heterogeneity in the subwavelength ($<\lambda/2$) domain. This may be detrimental since nanoscale heterogeneity may significantly contribute to the macroscopic properties of the sample. A remedy was proposed by Synge[1] in 1928 and practically realized by Pohl[2] in 1984. It consists of probing the electromagnetic field of the sample with an optical aperture with a radius smaller than the wavelength of the propagating wave emanating from the surface. To collect this near-field information, the aperture has to be kept in the close of the surface when the sample is scanned, since its intensity decreases exponentially with the aperture-to-surface separation. The so-called scanning near-field optical microscopy (SNOM or NSOM) is not limited by the diffraction limit since the near field does not propagate. The spatial resolution is then given by the diameter of the aperture, and SNOM paves the way for nanoscale spectroscopy.[3−7]

Several methods for creating small aperture probes have been developed. One of them consists of etching a fiber optic and coating the resulting tip with aluminum, except a small hole at the end of the tip. The coated fiber optic tip is then brought close to the surface of the sample, and the tip-to-sample distance is controlled by a feedback mechanism.[8,9] For instance, a dither piezo makes the tip oscillate at a resonance frequency, and the amplitude of vibration is monitored by imaging the shadow of the tip on a quadrant photodiode. When the tip enters the near-field condition, electromagnetic interaction between the tip and the sample produces a shear-force damping of the vibrational amplitude and shifting of the vibration frequency. The amplitude can be kept constant by controlling the tip-to-sample separation with a vertical piezo when the tip is horizontally scanned over the surface. It gives a shear-force topography of the scanned sample's area with a spatial resolution of now commonly $\sim\lambda/10$.[3−9] The main goal of SNOM is to couple this topographic information with an optical signal. Indeed, the setup can be properly designed to perform Raman,[10−12] nonlinear,[13] or fluorescence[14−32] spectroscopies. The tip can be used to illuminate the sample (illumination mode), collect the optical signal (collection mode), or both (illumination/collection mode). Near-field spectroscopy becomes a powerful method for identifying relationships between subwavelength heterogeneity and local optical and physicochemical properties. For instance, near-field Raman spectroscopy was applied to a sub-micrometric particle of $PbSO_4$ and revealed the presence of nanophases of $CuSO_4 \cdot 5H_2O$ that locally changed the tip−sample interaction.[12] Due to the small size of the nanophases, confocal Raman microscopy was not able to detect them.

When Raman scattering is not enhanced by plasmonic surfaces, its quantum efficiency is very low and the acquisition

* To whom correspondence should be addressed. Phone: (+33) 3 83 68 52 49. Fax: (+33) 3 83 27 54 44. E-mail: dossot@lcpme.cnrs-nancy.fr.
[†] UMR CNRS-UHP 7564.
[‡] CEA Saclay DEN/DANS/DPC/SCP.

10.1021/jp0607317 CCC: $33.50
Published on Web 05/18/2006

time for a near-field spectrum with a reasonable signal-to-noise ratio may be counted in hours. To obtain an optical image of the sample, a more efficient process may be preferable. Near-field fluorescence microscopy was thus developed[14−22] and is currently applied to a wide variety of samples, including biological material.[3,21,22,28] The fluorescence intensity at a given wavelength (generally, the wavelength of the emission maximum) is recorded during the scan, and the near-field fluorescence image of the surface is obtained. Using fluorescence intensity saves time but sometimes has a drawback of leading to artifacts. Indeed, fluorescence intensity can be modified by the tip−sample interaction if the tip is coated with aluminum. Fluorescence quenching or enhancement can be observed, and the efficiency of the process depends on the tip-to-sample distance.[7] Recording a near-field fluorescence spectrum at each pixel scanned may help to identify such artifacts since spectra contain more information than single-wavelength intensity. However, it is a time-consuming method, and its feasibility depends mainly on the sample. Since fluorescence lifetime was shown to be less sensitive to the tip-to-sample distance,[23,29] recording fluorescence decay kinetics may also be a convenient method of minimizing artifacts. Several groups have performed near-field time-resolved fluorescence spectroscopy using the time-correlated single-photon counting (TCSPC) method.[24−26,29−32] The excitation source was a mode-locked laser delivering picosecond or femtosecond pulses of light that were sent to the sample through the fiber optic tip (illumination mode). The fluorescence of the sample was then collected in the far field using the objective of an inverted microscope. An avalanche photodiode or a multichannel plate photomultiplier was used as a fast photodetector. In most of the studies, fluorescence decay kinetics or time-resolved spectra were obtained in a few regions of interest identified from either the topographic or fluorescence intensity images. Some studies report the measure of fluorescence decay kinetics at each pixel,[29,32] leading to a complete data set that can be subsequently exploited to give time-resolved images or decay kinetics for any region of interest (ROI).[32]

In our group, a near-field microscope has been developed and used to perform near-field Raman spectroscopy.[11,12] Starting with this home-built SNOM device, we now intend to develop a new setup to perform near-field time-resolved fluorescence spectroscopy. One of the envisaged applications concerns nuclear glass samples doped with Eu^{3+} cation. The fluorescence emission of the Eu^{3+} ion is on the microsecond to millisecond time scale.[33] Our approach was thus to develop a setup using either a continuous wave (CW) laser to obtain near-field fluorescence spectra with good spectral resolution or a nanosecond pulsed laser to obtain fluorescence decay kinetics in ROI determined from the shear-force topographic image. The setup should work with opaque and/or thick samples, and the collection mode was retained to make a versatile apparatus that can also probe solid−liquid interfaces. Besides, the design of the setup offers an opportunity to perform Raman and fluorescence spectroscopies in the same ROI, even though this combined approach is not exposed in this article. To test the validity of our approach for future research on nuclear glass samples, we used an aluminate glass that constitutes a reference matrix to model the aluminate environment that can be found in the SON68 glass.[34] This glass is nonradioactive and accurately reproduces the behavior and structure of the R7T7 nuclear glass that is used in France for the confinement of nuclear waste materials.[34] For the future storage of nuclear glass packages in deep geological layers, accurate evaluation of the physicochemical behavior of the glass submitted to various environmental conditions is required. This evaluation needs to characterize the surface of the model matrices using fluorescent probes that can model the migration of radionuclides through the glass matrix. The aluminate glass was thus doped with Eu^{3+} cations both as a fluorescent probe of the local chemical environment of the glass surface and as a good model of radioactive lanthanide cations.[33] The fact that the fluorescent probe is diluted into a glass matrix constitutes a challenge for SNOM time-resolved fluorescence spectroscopy (SNOM−TRFS) since fluorescence emitters are rather dispersed over the surface. The Eu^{3+}-doped aluminate glass then is a good sample to use in comparing the spectroscopic information obtained in the near field and far field with a CW or a pulsed laser as the excitation source.

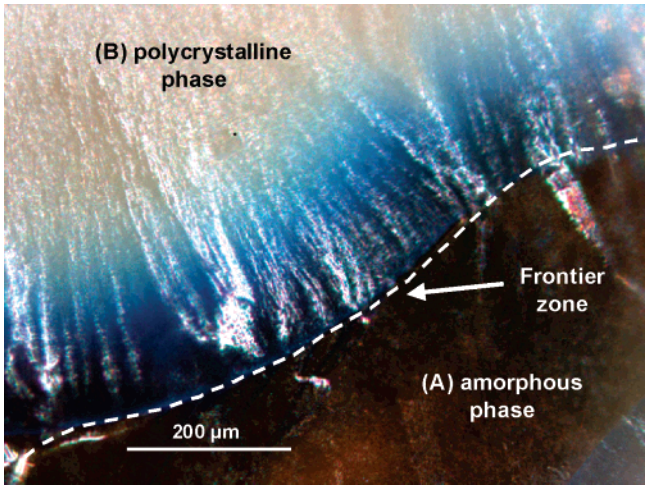

Figure 1. Optical image of the Eu^{3+}-doped glass showing the location of amorphous and polycrystalline phases where far-field fluorescence spectra were recorded.

2. Materials and Methods

2.1. Glass Sample. The aluminate glass is one of the four model matrices of the SON68 glass. Its chemical composition is as follows[34] (in weight percent): 45.0% Al_2O_3, 53.5% CaO, and 1.5% Eu_2O_3. The sample was prepared by mixing the oxide powders in the appropriate proportions and then melting them at 1500 °C in a crucible. After a period at 700 °C, a cooling of the glass at room temperature was carried out. During this cooling step, some parts of the glass undergo a crystallization process that creates local polycrystalline areas in the bulk and at the surface of the sample. Figure 1 is an optical image of the sample that shows an interesting region where both the amorphous and polycrystalline phases are present. Due to the size of visible heterogeneities (width of >10 μm) under an optical microscope, it was possible to perform far-field fluorescence measurements at either the amorphous or the polycrystalline areas. The question was whether the near-field microscope was able to explore the frontier between the two phases and then to reveal the heterogeneity of the sample at a sub-micrometric scale. Due to the presence of the two different phases, the Eu^{3+}-doped glass constitutes a very good sample for testing the validity of the information collected in the near field compared to the data obtained in the far field.

2.2. Far-Field Time-Resolved Fluorescence Spectroscopy. Time-resolved fluorescence spectroscopy was carried out in the far field following the setup of Figure 2. The excitation source was a pulsed Nd:YAG laser emitting at 532 nm, with a pulse fwhm of 5 ns and an energy of 250 μJ/pulse. The laser beam was focused on a SMA fiber by a SMA coupler. The light going

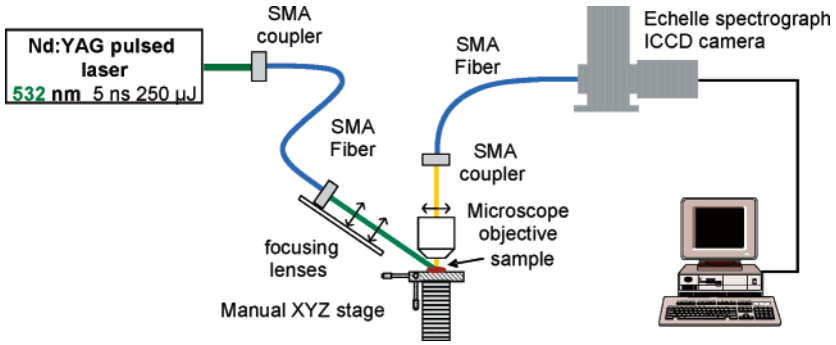

Figure 2. Experimental setup for TRFS experiments in the far field.

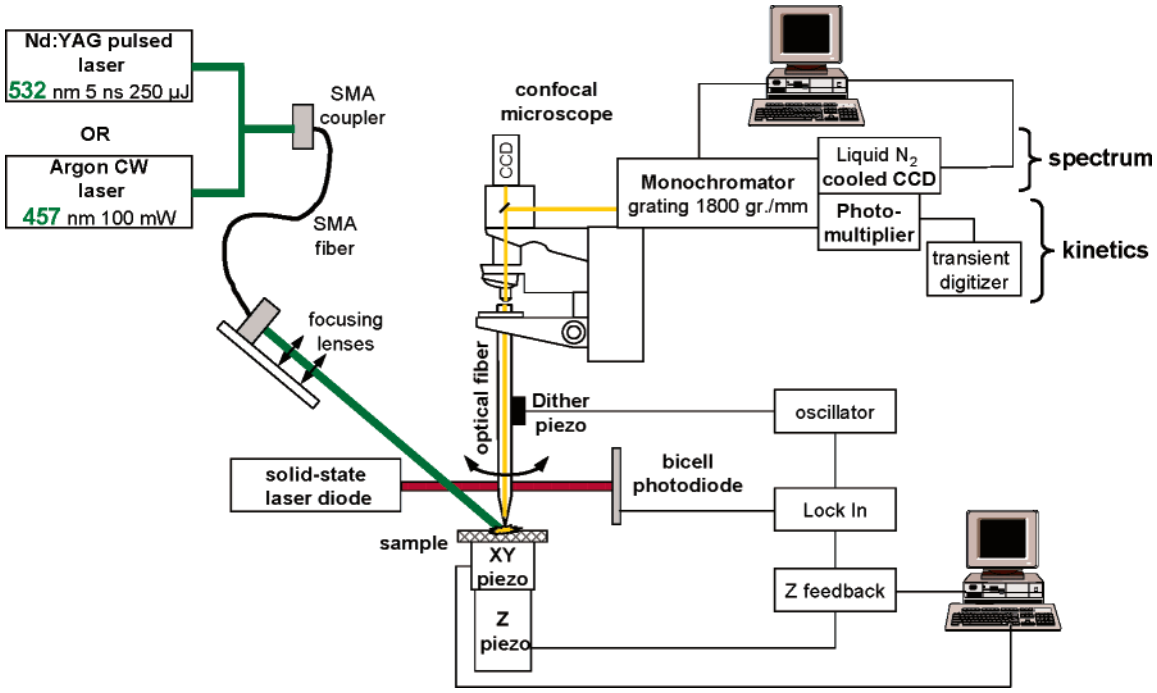

Figure 3. Experimental setup for SNOM−TRFS experiment.

out of the SMA fiber was focused on the glass sample by lenses. The angle between the laser beam and the vertical was approximately 30°. The aluminate glass sample was placed on a manual XYZ stage under a microscope objective that collected in the far field the fluorescence of the excited sample. Another SMA fiber was used to project the fluorescence light on a spectrograph (PI Mare from Princeton Instrument) and an intensified CCD camera (PI Echelle spectrograph SE200 from Princeton Instrument). The camera was triggered on the Pockels' cell of the laser to synchronize the two apparatus. A computer was used to control the ICCD, acquire the time-resolved fluorescence spectra, and fit the fluorescence decay kinetics.

2.3. Near-Field Fluorescence Spectroscopy. Near-field fluorescence spectroscopy was performed using the setup presented in Figure 3. The excitation source and, correspondingly, the detector were different in either time-resolved or spectral measurements. For measurement of near-field fluorescence decay kinetics, the same pulsed Nd:YAG laser used in the far field (Figure 2) was selected and the detector was a photomultiplier placed beyond a monochromator and a slit. A transient digitizer stored the signal of the photomultiplier before mathematical analysis was carried out on a computer. For spectral measurements, either the pulsed Nd:YAG laser or a CW argon laser emitting at 457 nm, with a power of 200 mW, was used. The detector was a CCD camera cooled by liquid N_2 placed after a Jobin-Yvon T64000 spectrograph.

The excitation beam (either pulsed or CW) was focused on the sample with the help of a SMA fiber and lenses. The near-field microscope was the same as that previously described.[11,12] Briefly, the fiber optic tip was oscillating at the resonant frequency by a dither piezo coupled to an electrical oscillator. The detection of the tip vibration was realized by illuminating the tip with a solid-state laser diode at 685 nm. The shadow of the tip was imaged on a bicell photodiode that produced an electric signal oscillating at the same frequency as the tip and whose amplitude was proportional to the amplitude of the tip vibration. When the tip entered the near-field condition of the sample, a shear force was probed by the tip and a change in the frequency and amplitude of vibration was recorded. A lock-in amplifier compared the excitation signal of the dither piezo with the signal given by the photodiode. The amplitude of vibration was kept at a chosen value, and the lock-in amplifier was used as a feedback controller of the Z piezo under the sample. The Z piezo was submitted to a tension adequate to keep the amplitude of the tip's vibration constant. Thus, after a horizontal XY scan of the sample, a shear-force topography of the surface probed by the tip was obtained.

The fiber optic tip in the near-field condition was used to collect the fluorescence emitted by the sample. The fiber optic was coupled to a confocal microscope. A CCD camera at room temperature placed just ahead of the microscope was used to obtain a visual image of the sample. The fluorescence light was

then spectrally decomposed by a monochromator equipped with a grating with 1800 grooves/mm. The monochromator and the slits of the Jobin-Yvon T64000 spectrograph were controlled by a computer that also acquires the numeric signal of the cooled CCD camera for spectral measurements. For time-resolved measurements, the photomultiplier was directly inserted after the monochromator and the exit slit and the signal was collected by the transient digitizer. To verify that the fluorescence was properly collected in the near field, the fluorescence intensity at a given wavelength was observed versus the voltage applied on the Z piezo (i.e., the tip-to-sample separation). It was found that the intensity dramatically decreased when the tip-to-sample separation increased, in accordance with the exponential decay predicted by the theory[3−6] (data not shown).

2.4. Fitting Procedure of the Fluorescence Decay Kinetics. Commercial software (Origin version 6.1 from Microcal Software Inc.) is used to adjust a pulse curve to the kinetic data obtained in the far field and in the near field. The pulse mathematical expression is given in eq 1

$$y = y_0 + A\left[1 - e^{\frac{-(t - t_0)}{\tau_1}}\right]e^{-(t-t_0)/\tau_2} \qquad (1)$$

where y is the fluorescence intensity, A the amplitude of the signal, τ_1 the rise time, and τ_2 the fluorescence decay time. y_0 and t_0 (fluorescence signal at time zero) are fixed to zero. The rise time (τ_1) is determined by recording only the laser pulse with the monochromator set at 532 nm and subsequently fixed to the value so obtained, i.e., 0.30 ms in the near field (mainly due to the fact that the photomultiplier signal is subjected to a 1 MΩ resistance to increase the signal voltage) and 7.8 μs in the far field (using a 10 kΩ resistance to collect the signal from the ICCD detector). The adjusting parameters of the fit are thus A and τ_2, and their values are retrieved by using a nonlinear Marquardt−Levenberg algorithm.

3. Results and Discussion

3.1. Far-Field Fluorescence Spectra. The optical image in Figure 1 shows the amorphous and polycrystalline phases of the aluminate glass. The heterogeneity of the sample is thus obvious at this almost macroscopic scale, and the frontier region between the two phases offers the opportunity to search heterogeneities at different spatial scales. Comparison of the spectral information collected either in the far field or in the near field on this frontier region should therefore be valuable in estimating the spectral accuracy of the SNOM setup and the potential effect of the tip−sample interaction on the Eu^{3+} fluorescence. Figure 4 shows far-field fluorescence spectra collected in the amorphous phase (spectrum A) or in the polycrystalline phase (spectrum B) after excitation at 532 nm with the pulsed Nd:YAG laser. The two spectra exhibit four principal emission bands assigned to the luminescence of the Eu^{3+} cation from its excited $^5D_0$ electronic level to the four ^7F_J ($J = 1-4$) levels.[33−42] In the case of spectrum A, the four $^5D_0 \rightarrow {}^7F_J$ emission bands are broad and seem to be composed of several emission lines. This is more obvious for spectrum B, especially concerning the $^5D_0 \rightarrow {}^7F_1$ and $^5D_0 \rightarrow {}^7F_2$ transitions which are more structured with individual peaks. Table 1 compiles the wavelength of the main peaks that can be observed in the two spectra of Figure 4. Since the $^5D_0$ level has a J of 0, the different emission lines essentially come from the Stark splitting of the ^7F_J ($J = 1-4$) levels by the crystal field surrounding Eu^{3+} cations. As the europium cation is included within a solid matrix, we cannot exclude the possibility that some vibronic lines contribute to the spectral width, but their intensity should be very low compared to that of the pure electronic transitions.[37] The fact that spectrum B has more structured $^5D_0 \rightarrow {}^7F_1$ and $^5D_0 \rightarrow {}^7F_2$ emission bands (in the spectral ranges of 580−600 and 600−630 nm, respectively) than spectrum A may result from a higher crystal field effect in the polycrystalline region that would increase the Stark splitting of the $^7F_1$ and $^7F_2$ levels. Indeed, three peaks are observed for the $^5D_0 \rightarrow {}^7F_1$ transition, and at least four peaks are visible for the $^5D_0 \rightarrow {}^7F_2$ transition. Table 1 also reports the ratio R of the integrated fluorescence intensity between the $^5D_0 \rightarrow {}^7F_2$ and $^5D_0 \rightarrow {}^7F_1$ emission bands. Since the $^5D_0 \rightarrow {}^7F_2$ transition is an electrically allowed transition, it is very sensitive to the surroundings of the Eu^{3+} cation, whereas the magnetically allowed $^5D_0 \rightarrow {}^7F_1$ transition is almost not influenced. Consequently, R provides information about the breaking of centro-symmetry and the degree of disorder around the europium cation.[34−42] For spectrum A obtained in the amorphous phase, $R = 7.69 \pm 0.12$, in excellent agreement with the previously reported value of 7.55 in ref 34. This high value for R indicates that the symmetry around Eu^{3+} cations in the amorphous phase is low and the degree of disorder important.[34] With regard to the polycrystalline region, spectrum B leads to a value of 4.08 ± 0.05 for R, which also indicates that centro-symmetry is broken but the degree of disorder is not as important as for the amorphous phase. A value of 4.08 for R can be compatible with C_{2v} symmetry around the europium cations, a hypothesis that also agrees well with the important Stark splitting observed in spectrum B. To confirm this hypothesis, fluorescence line narrowing experiments should be performed to excite selectively the Eu^{3+} cations localized in these sites.[34−42] Future work will be devoted to this matter. Although the interpretation remains speculative, the important result is that the amorphous and polycrystalline phases can clearly be distinguished by their spectral features in the fluorescence emission of the Eu^{3+} cations.

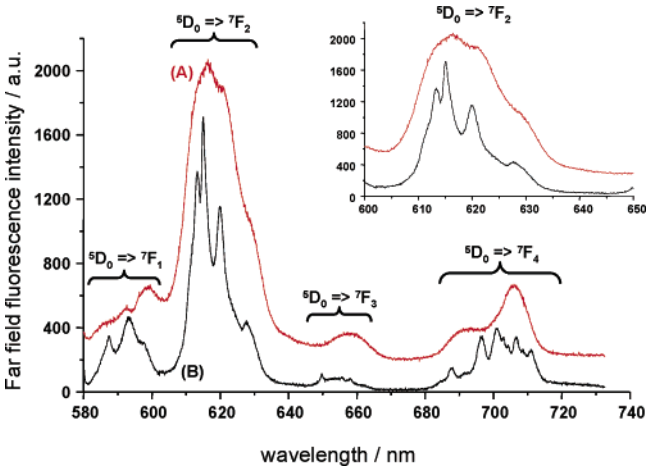

Figure 4. Far-field fluorescence spectra of the Eu^{3+}-doped glass sample after excitation with the Nd:YAG pulsed laser at 532 nm in amorphous (A) and polycrystalline (B) phases depicted in Figure 1.

The far-field fluorescence spectra were collected using a 100× microscope objective to achieve a spatial resolution of ~1 μm. However, Figure 1 shows that the frontier region between the two phases exhibits an important relief. Spatially resolved X-ray photoelectron spectroscopy (with a lateral resolution of ~10 μm) has been performed in this region and has evidenced that thin (<100 nm) slabs of amorphous glass sometimes recover crystalline areas (data not shown). Since the axial resolution of the confocal microscope is not sufficient for

TABLE 1: Spectral Features of the Fluorescence Emission Spectra of the Eu^{3+}-Doped Glass with (i) Pulsed Nd:YAG 532 nm Laser Excitation and Collection in the Far Field (spectra A and B), (ii) Continuous Wave Argon Laser 457 nm Excitation and Collection in the Near Field (spectra A′ and B′), and (iii) Pulsed Nd:YAG 532 nm Laser Excitation and Collection in the Near Field (spectra C and D)[a]

	spectrum A		spectrum A′		spectrum C
transition assignment	relative area	contribution wavelengths (nm)	relative area	contribution wavelengths (nm)	contribution wavelengths (nm)
$^5D_0 \rightarrow {}^7F_1$	0.130	592.6	0.128	591.8 (s)	nd
		598.4		598.4	nd
$^5D_0 \rightarrow {}^7F_2$	1	616.6 (max)	1	616.3 (max)	615.1 (max)
		621 (s)		621 (s)	621 (s)
	$R = 7.69 \pm 0.12$	629 (s)	$R = 7.81 \pm 0.18$	629 (s)	629 (s)
	spectrum B		spectrum B′		spectrum D
transition assignment	relative are	contribution wavelengths (nm)	relative area	contribution wavelengths (nm)	contribution wavelengths (nm)
$^5D_0 \rightarrow {}^7F_1$	0.245	587.4	0.260	587.5	nd
		593.4		593.6	nd
$^5D_0 \rightarrow {}^7F_2$	1	613.3	1	613.4	612.9
		614.1 (max)		614.9 (max)	614.7 (max)
	$R = 4.08 \pm 0.05$	620.1	$R = 3.85 \pm 0.1$	620.0	619.6
		627.7		627.5 (s)	627.3 (s)

[a] s, shoulder; max, maximum of emission. The relative area columns contain the relative integrated fluorescence intensity of the emission band associated with the electronic transitions and normalized to the $^5D_0 \rightarrow {}^7F_2$ transition. They also report the R values of these relative intensities.

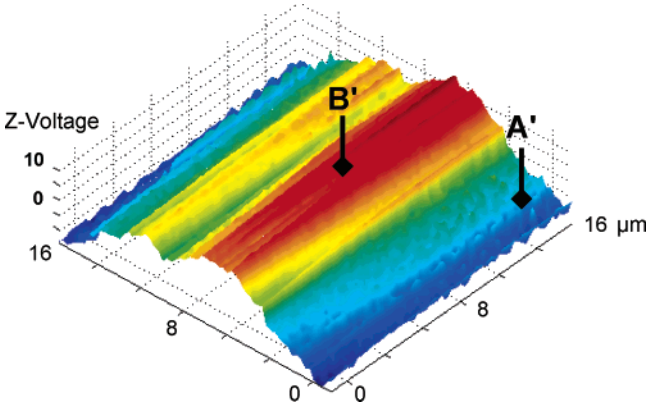

Figure 5. Shear-force topography of a 16 μm × 16 μm area (128 × 128 pixels) of the Eu^{3+}-doped glass sample in the frontier region between the amorphous and polycrystalline phases. Sites A′ and B′ correspond to the near-field fluorescence spectra obtained with the CW argon laser exciting at 457 nm. Site B′ corresponds to a region of the sample where the tip−sample interaction is strong, as opposed to that in site A′.

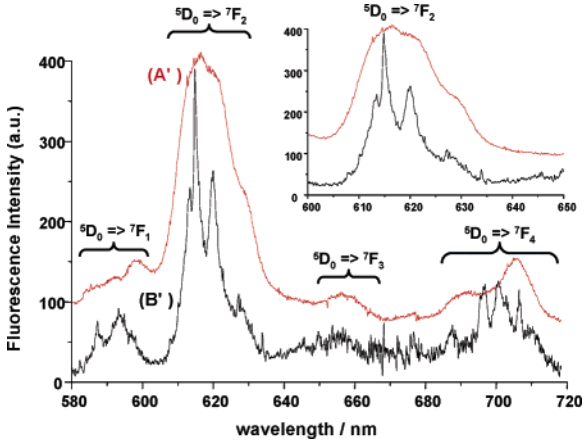

Figure 6. Examples of two near-field fluorescence spectra taken at site A′ (red) and B′ (black) defined in Figure 5 with the CW argon laser exciting at 457 nm. The inset shows an expand region between 600 and 650 nm that can be compared with the spectra reported in Figure 4 (far-field spectra). Spectrum A′ is shifted for the sake of clarity.

optical detection of such slabs, the heterogeneity of the frontier region is very difficult to investigate with the confocal microscope. Therefore, it is interesting to benefit from the submicrometric spatial resolution of the SNOM device in performing near-field fluorescence spectroscopy in this part of the aluminate glass sample.

3.2. Near-Field Fluorescence Spectra. The fiber optic tip of the SNOM device was localized in the frontier region between the amorphous and polycrystalline regions, and a shear-force topography of a rather wide area (16 μm × 16 μm) was recorded. The resulting topography is given in Figure 5. This part of the glass sample is characterized by important topographical relief. Two sites were selected from the topographical image to collect near-field fluorescence spectra. Site A′ (Figure 5) was chosen in a zone where the tip−sample interaction was weak, whereas site B′ was chosen at the top of the relief observed in Figure 5. To have the best signal-to-noise (S/N) ratio, the near-field fluorescence spectra were recorded in sites A′ and B′ by exciting the glass sample with the CW argon laser at 457 nm. It is also a means of testing if the tip−sample interaction might disturb the spectral information compared to far-field measurements. The corresponding spectra are given in Figure 6. The most striking result is the similarity between spectra A and A′ and between spectra B and B′ despite the change in the excitation wavelength from 532 nm in Figure 4 to 457 nm in Figure 6. This result suggests that site A′ corresponds to an amorphous zone and site B′ to a (poly)-crystalline zone. It also indicates that the tip does not perturb the fluorescence spectrum since the features are the same in the far and near field. When the glass is illuminated at 457 nm, the europium cation is excited to the $^5D_2$ level, whereas illumination at 532 nm excites Eu^{3+} to its $^5D_1$ level. At room temperature, both of these excited states are quickly deactivated by internal conversion to the excited $^5D_0$ state.[35] The fact that spectra in Figure 6 are almost identical to the spectra in Figure 4 confirms that the fluorescence emission comes exclusively from the $^5D_0$ level. Table 1 gathers the features of spectra A′ and B′, and one can clearly see the similarities with spectra A and B, respectively. The R values are almost the same as those previously obtained in the far field. Amorphous site A′ is still characterized by a high degree of disorder ($R = 7.81 \pm 0.18$)

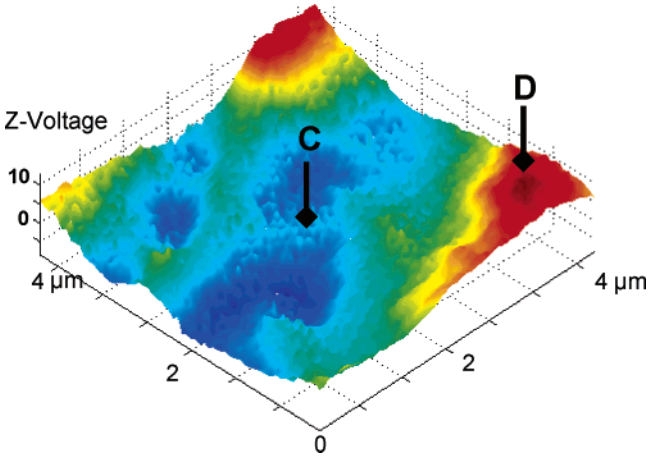

Figure 7. Shear-force topography of a 4 μm × 4 μm area (128 × 128 pixels) of the Eu^{3+}-doped glass sample in the frontier region between the amorphous and polycrystalline phases. Sites C and D are for subsequent near-field spectral and kinetics measurements with the pulsed Nd:YAG laser as the excitation source at 532 nm.

even in the near field. Site B′ has a value of 3.85 ± 0.1 for *R*, which is closed to the far-field value of 4.08 ± 0.05 obtained previously. The slight decrease in *R* may be due to a decrease in the S/N ratio in near-field spectrum or to a localized slight change of symmetry around Eu^{3+} cations. Since the surface probed in the near field is considerably smaller than that in the far field, the distribution of sites can be narrowed in the near field, possibly yielding a lower *R* value.

3.3. Near-Field Time-Resolved Fluorescence Spectroscopy. The topographical scan reported in Figure 5 covers a rather wide area of the surface. To see if the near-field microscope is able to detect spectral heterogeneities at a smaller spatial scale, several less extended topographic scans have been performed within the frontier region between the amorphous and polycrystalline phases. Figure 7 gives an interesting example of such scans that covers a 4 μm × 4 μm area. It can be seen that some topographical relief is present at this spatial scale. The SNOM topography reveals heterogeneities at a sub-micrometric scale that could not be optically detected in the far field. It is thus interesting to obtain fluorescence spectra in sites where the tip−sample interaction changes. Near-field time-resolved fluorescence spectroscopy was performed in this part of the glass sample using the pulsed Nd:YAG laser at 532 nm to excite europium cations. As a preliminary investigation, near-field fluorescence spectra were recorded at several sites using the pulsed laser to compare with the near-field spectra obtained with CW laser excitation. The detector was thus the N_2-cooled CCD camera of the Jobin-Yvon T64000 spectrometer. The results were as follows. When a topographical relief is present, like in site D indicated in Figure 7, the $^5D_0 \rightarrow {}^7F_2$ emission band was structured as observed above for the polycrystalline phase. By contrast, when the tip−sample interaction force is low as in site C (Figure 7), the $^5D_0 \rightarrow {}^7F_2$ emission band was broad and less structured as for the amorphous phase spectra previously discussed. Figure 8 gives the corresponding spectra for sites C and D. Though the S/N ratio is lower, the pulsed laser setup allows us to monitor the fluorescence spectra with the cooled CCD camera to select the sites on the sample that have interesting spectral features. The spectra in Figure 8 show that the tip−sample interaction does not change the spectral features, but one can wonder if the fluorescence kinetics would be modified in the near field. Subsequent fluorescence decay measurements have been taken. As an example, Figure 9 reports the fluorescence decay kinetics obtained in sites C and D using

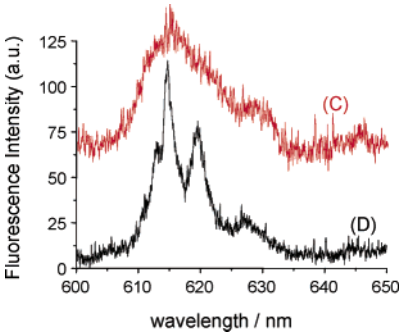

Figure 8. Examples of two near-field fluorescence spectra taken at sites C and D defined in Figure 7. Excitation is provided by the pulsed Nd:YAG laser at 532 nm, and the N_2-cooled CCD camera is the spectral detector.

a photomultiplier directly placed after the monochromator slit. For comparison, Figure 9 also reports the fluorescence decay signals obtained in the far field and corresponding to spectra A and B of Figure 4. The emission wavelength was 615 nm in all cases, and the experimental data were fitted via eq 1. The resulting rise time (τ_1) and fluorescence decay time (τ_2) are indicated in each case. These results show that the observation of a structured emission band for the $^5D_0 \rightarrow {}^7F_2$ transition is associated with a higher τ_2 value. The near-field values of τ_2 are lower than those in the far field: $\tau_2 = 0.64 \pm 0.09$ ms instead of 0.98 ± 0.03 ms for the amorphous site, and $\tau_2 = 0.96 \pm 0.07$ ms instead of 2.30 ± 0.03 ms for the polycrystalline site. This may be due to a slight quenching effect of the aluminum-coated fiber optic tip. Besides, the S/N ratio of the near-field fluorescence decay kinetics is markedly lower than that in the far field, and that can affect the value of the fitting parameters of eq 1. These results confirm the interest in performing time-resolved measurements since the tip−sample interaction is revealed through an effect on the decay kinetics but not on the fluorescence spectra. Although some improvements have to be carried out on the experimental setup to tentatively increase this S/N ratio, the SNOM−TRFS experiments performed on the aluminate glass sample confirm that spectral and kinetic heterogeneities are associated with topographic relief at a sub-micrometric spatial scale. Thus, our approach for future work on nuclear glass is validated.

3.4. Local Heterogeneities on the Aluminate Glass Sample. The comparison of fluorescence spectra of Figures 4, 6, and 8 and the *R* values reported in Table 1 reveals that the fiber optic tip does not significantly perturb the measurement of fluorescence emission spectra. Near-field experiments show that the frontier region between the macroscopic amorphous and polycrystalline phases of the glass sample also contains heterogeneities at a sub-micrometric spatial scale. These heterogeneities appear as simultaneous changes in topography (polycrystalline areas appear to interact more strongly with the optic fiber tip), fluorescence emission (an increase in Stark splitting and a lower *R* value for polycrystalline sites), and kinetics (polycrystalline areas have a longer fluorescence decay time at 615 nm). The chemical environment surrounding the Eu^{3+} cations in the polycrystalline sites seems to be compatible with C_{2v} symmetry as shown by the Stark splitting and the value of *R*. The emission peaks reported in Table 1 for spectra B, B′, and D could be compatible with the formation of partially hydroxylated europium cation with Eu−O−H bonds.[42] The europium cation may displace Al^{3+} cation in the glass matrix, and the crystallization process may have led to the partial hydroxylation of the surface. If such a phenomenon can be invoked, it would also modify the shear-force interaction between the silica tip

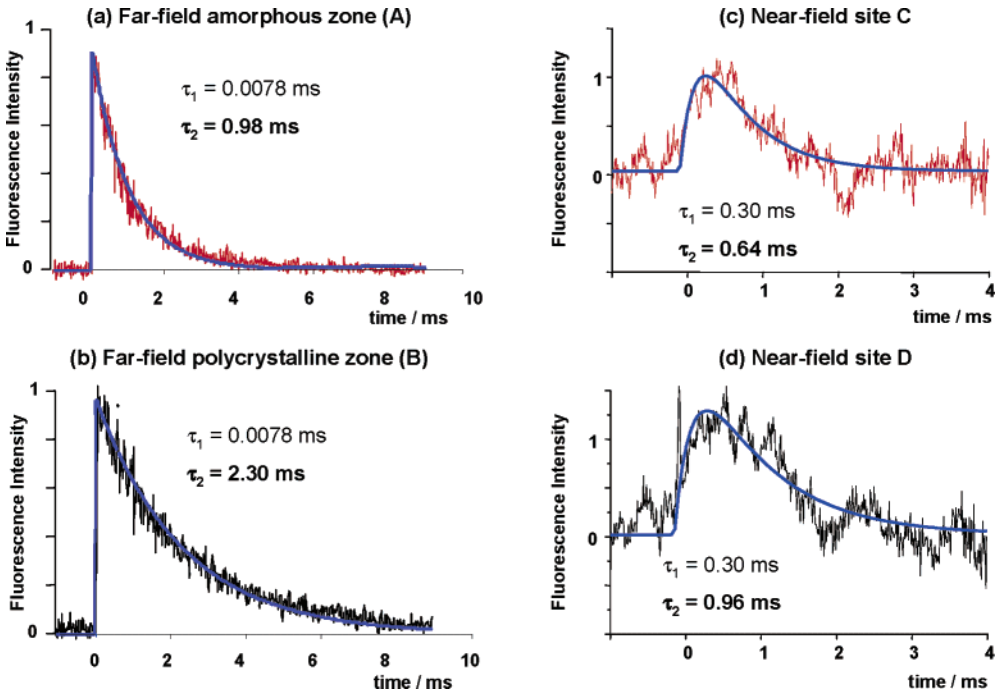

Figure 9. Far-field and near-field fluorescence decay kinetics obtained at 615 nm. Far-field kinetics are taken in the amorphous (A) and polycrystalline (B) phases, and near-field kinetics are recorded at sites C and D defined in Figure 7. In all cases, excitation is obtained by the pulsed Nd:YAG laser at 532 nm. For near-field measurements, the detector is a photomultiplier. Blue lines are least-squares fits by eq 1 with the reported values of rise time (τ_1) and decay time (τ_2).

and the surface. To validate or reject these speculative explanations, future work will be done using a dye laser to excite selectively the Eu^{3+} cations surrounded by different chemical environments. The fluorescence spectra thus obtained will be analyzed through spectral deconvolution to unravel the contributions to the different electronic transitions. The spectral analysis will be useful in asserting the symmetry environment of europium cations.[34−38] We thus intend to couple the SNOM setup with fluorescence line narrowing experiments to be more selective in terms of the chemical information generated by the luminescence spectrum of Eu^{3+} cation and to benefit from the sub-micrometric spatial resolution of the SNOM.

4. Conclusion

Near-field fluorescence spectroscopy has been applied to an aluminate glass sample doped with Eu^{3+} cation as a fluorescent probe of its surrounding environment. The surface of the glass was found to be rather heterogeneous at both microscopic and sub-micrometric spatial scales. Near-field fluorescence spectra as well as fluorescence decay kinetics reveal that two environments for the Eu^{3+} cation exist. One corresponds to a very disordered environment in an amorphous matrix, and the second is a more ordered environment within a polycrystalline matrix. The SNOM device revealed sub-micrometric heterogeneities that confocal microscopy was not able to reveal due to the peculiar topography of the frontier region between the two phases. Subsequent SNOM−TRFS measurements confirmed the interest in recording fluorescence decay kinetics to unravel tip−sample interaction by the change in the fluorescence decay time. A more thorough investigation will be conducted on this glass sample to precisely determine the europium environment in both the amorphous and polycrystalline phases. Furthermore, as the near-field signals come mainly from the surface due to the exponential decay of the nonpropagative electromagnetic field, the method would be valuable in studying the effect of solution leaching of glass surfaces. The leaching process may amplify the surface heterogeneities and lead to local physicochemical environments that could be probed using Eu^{3+} cations. Finally, the SNOM−TRFS technique could also be applied to oxide surfaces sorbed with Eu^{3+} cations from solutions with different physicochemical conditions in studying the potential retention of lanthanides by such surfaces at the molecular level, a subject that will have a strong impact on the future storage of nuclear waste.

Acknowledgment. We thank Patrick Jollivet (LCLT, CEA Valrhô, Bagnols-sur-Cèze, France) for giving us the great opportunity to work with Eu^{3+}-doped glass samples.

References and Notes

(1) Synge, E. H. *Philos. Mag.* **1928**, *6*, 356.
(2) Pohl, D. W.; Denk, W.; Lanz, M. *Appl. Phys. Lett.* **1984**, *44*, 651.
(3) Dunn, R. C. *Chem. Rev.* **1999**, *99*, 2891.
(4) Yoshikawa, H.; Masuhara, H. *J. Photochem. Photobiol., C* **2000**, *1*, 57.
(5) Hsu, J. W. P. *Mater. Sci. Eng., R* **2001**, *33*, 1.
(6) Kirstein, S. *Curr. Opin. Colloid Interface Sci.* **1999**, *4*, 256.
(7) Hecht, B.; Sick, B.; Wild, U. P.; Deckert, V.; Zenobi, R.; Martin, O. J. F.; Pohl, D. W. *J. Chem. Phys.* **2000**, *112*, 7762.
(8) Betzig, E.; Finn, P. L.; Weiner, J. S. *Appl. Phys. Lett.* **1992**, *60*, 2484.
(9) Toledo-Crow, R.; Yang, P. C.; Chen, Y.; Vaez-Iravani, M. *Appl. Phys. Lett.* **1992**, *60*, 2957.
(10) Ayars, E. J.; Jahncke, C. L.; Paesler, M. A.; Hallen, H. D. *J. Microsc.* **2001**, *202*, 142.
(11) Grausem, J.; Humbert, B.; Spajer, M.; Courjon, D.; Burneau, A.; Oswalt, J. *J. Raman Spectrosc.* **1999**, *30*, 833.
(12) Humbert, B.; Grausem, J.; Courjon, D. *J. Phys. Chem. B* **2004**, *108*, 15714.
(13) Schaller, R. D.; Johnson, J. C.; Wilson, K. R.; Lee, L. F.; Haber, L. H.; Saykally, R. J. *J. Phys. Chem. B* **2002**, *106*, 5143.
(14) Nguyen, T.-Q.; Schwartz, B. J.; Schaller, R. D.; Johnson, J. C.; Lee, L. F.; Haber, L. H.; Saykally, R. J. *J. Phys. Chem. B* **2001**, *105*, 5153.
(15) Huser, T.; Yan, M. *Synth. Met.* **2001**, *116*, 333.
(16) Stevenson, R.; Granström, M.; Richards, D. *Phys. Status Solidi B* **1999**, *215*, 65.
(17) Nagahara, T.; Imura, K.; Okamoto, H.; Oguro, A.; Imahori, H. *J. Phys. Chem. B* **2005**, *109*, 19839.

(18) Kim, J. M.; Ohtani, T.; Muramatsu, H. *Surf. Sci.* **2004**, *549*, 273.
(19) Donthu, S. K.; Pan, Z.; Shekhawat, G. S.; Dravid, V. P.; Balakrisnan, B.; Tripathy, S. *J. Appl. Phys.* **2005**, *98*, 024304.
(20) Vanden Bout, D. A.; Kerimo, J.; Higgins, D. A.; Barbara, P. F. *J. Phys. Chem.* **1996**, *100*, 11843.
(21) Burgos, P.; Yuan, C.; Viriot, M. L.; Johnston, L. J. *Langmuir* **2003**, *19*, 8002.
(22) Kim, J. M.; Muramatsu, H.; Lee, H. Y.; Kawai, T. *FEBS Lett.* **2003**, *19*, 8002.
(23) Pagnot, T.; Barchiesi, D.; Tribillon, G. *Appl. Phys. Lett*. **1999**, *75*, 4207.
(24) Miura, A.; Yanagawa, Y.; Tamai, N. *J. Microsc.* **2001**, *202*, 425.
(25) Nabetani, Y.; Yamasaki, M.; Miura, A.; Tamai, N. *Thin Solid Films* **2001**, *393*, 329.
(26) Aoki, H.; Ito, S. *J. Phys. Chem. B* **2001**, *105*, 4558.
(27) Veerman, J. A.; Levi, S. A.; van Veggel, F. C. J. M.; Reinhoudt, D. N.; van Hulst, N. F. *J. Phys. Chem. A* **1999**, *103*, 11264.
(28) Garcia-Parajo, M. F.; Veerman, J. A.; Segers-Nolten, G. M. J.; de Grooth, B. G.; Greve, J.; van Hulst, N. F. *Cytometry* **1999**, *36*, 239.
(29) Cadby, A.; Dean, R.; Fox, A. M.; Jones, R. A. L.; Lidzey, D. G. *Nano Lett*. **2005**, *5*, 2232.
(30) Reid, P. J.; Higgins, D. A.; Barbara, P. F. *J. Phys. Chem*. **1996**, *100*, 3892.
(31) Kwak, E.-S.; Kang, T. J.; Vanden Bout, D. A. *Anal. Chem*. **2001**, *73*, 3257.
(32) Kwak, E.-S.; Vanden Bout, D. A. *Anal. Chim. Acta* **2003**, *496*, 259.
(33) Plancque, G.; Moulin, V.; Toulhoat, P.; Moulin, C. *Anal. Chim. Acta* **2003**, *478*, 11.
(34) Thévenet, F.; Panczer, G.; Jollivet, P.; Champagnon, B. *J. Non-Cryst. Solids* **2005**, *351*, 673.
(35) Reisfeld, R.; Velapoldi, R. A.; Boehm, L. *J. Phys. Chem*. **1972**, *76*, 1293.
(36) Kushida, T. *J. Lumin.* **2002**, *100*, 73.
(37) Fu, Z.; Zhou, S.; Yu, Y.; Zhang, S. *J. Phys. Chem. B* **2005**, *109*, 23320.
(38) Lochhead, M. J.; Touryan, L.; Vogel, V. *J. Phys. Chem. B* **1999**, *103*, 3411.
(39) Annapurna, K.; Das, M.; Kundu, P.; Dwivedi, R. N.; Buddhudu, S. *J. Mol. Struct.* **2005**, *741*, 53.
(40) Zhang, Y.; Wany, M. *Mater. Lett.* **1999**, *41*, 149.
(41) Alombert-Goget, G.; Gaumer, N.; Obriot, J.; Rammal, A.; Chaussedent, S.; Monteil, A.; Portales, H.; Chiasera, A.; Ferrari, M. *J. Non-Cryst. Solids* **2005**, *351*, 1754.
(42) Pointeau, I.; Piriou, B.; Fedoroff, M.; Barthes, M.-G., Marmier, N.; Fromage, F. *J. Colloid Interface Sci.* **2001**, *236*, 252.